CHALMERS

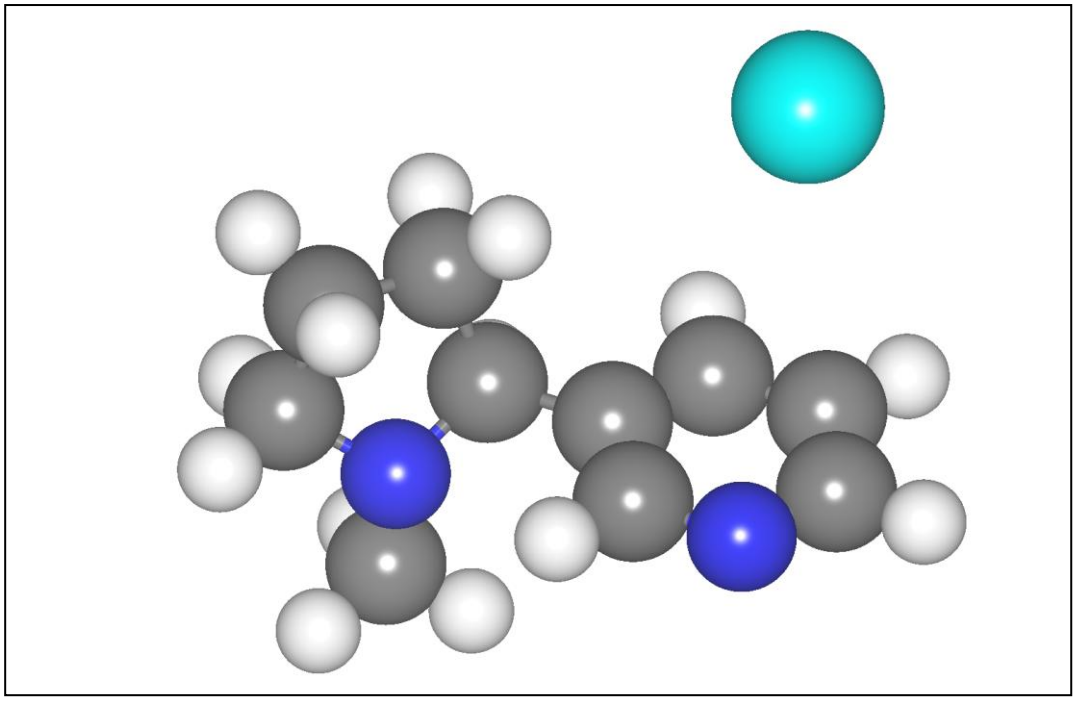

Capturing radon on tobacco smoke

A non-empirical study of the van der Waals binding of radon on smoke

Master of Science Thesis in Fundamental Physics

MAGNUS SANDÉN

Supervisor: Per Hyldgaard

Microtechnology and Nano Science, MC2
Bio-Nano Physics Laboratory
CHALMERS UNIVERSITY OF TECHNOLOGY
Göteborg, Sweden, 2011

Thesis for the Degree of Master of Science in Fundamental Physics

Capturing radon on tobacco smoke

A non-empirical study of the van der Waals binding of radon on smoke

Magnus Sandén

Department of Microtechnology and Nanoscience, MC2
BioNano Systems Laboratory
CHALMERS UNIVERSITY OF TECHNOLOGY
Göteborg, Sweden 2011

Capturing radon on tobacco smoke
A non-empirical study of the van der Waals binding of radon on smoke
Magnus Sandén

Thesis for the Degree of Master of Science in Fundamental Physics

© Magnus Sandén, 2011

Department of Microtechnology and Nanoscience, MC2
BioNano Systems Laboratory
CHALMERS UNIVERSITY OF TECHNOLOGY
SE-412 96 Göteborg
Sweden www.chalmers.se Tel. +46-(0)31 772 1000

Cover: Radon atom adsorbed on nicotine. Picture created using VESTA [1].
Printed by Reproservice
Göteborg, Sweden 2011

Capturing radon on tobacco smoke

A non-empirical study of the van der Waals binding of radon on smoke

Magnus Sandén
Department of Michrotechnology and Nanoscience, MC2, Chalmers University of Technology

Abstract

Radon is one of the largest causes for lung cancer in the world. In fact, it is second only to smoking. It has been observed that tobacco smoking increases the risks of radon-induced lung cancer, but there does not appear to be any theory that quantitatively describes why this is. This thesis is a study of a possible reason for this increase in mortality.

I have investigated if and how radon atoms adsorb onto some molecules present in tobacco smoke and other types of smoke. My study can therefore also help to develop an understanding of possible radon-associated health effects that may follow from enjoying an open fireplace. If radon does adsorb onto the smoke it may increase the likelihood of these radioactive atoms decaying in the lungs and depositing their daughter nuclei there. Most of the daughter nuclei are radioactive and of them at least lead is also toxic.

The investigation was done through electronic structure calculations using density functional theory. I have chosen a non-empirical method because there are not many experiments on radon interactions. The van der Waals density functional was used to account for the van der Waals interactions.

Adsorbtions of between 70 meV and 156 meV were found on all investigated molecules from the smoke. Large polycyclic aromatic hydrocarbons gave the strongest adsorbtion. In a trend study with different noble gas atoms, bigger atoms adsorbed more strongly, including radon which adsorbed most strongly.

The thesis includes an overview of the theory behind the density functional theory used in the calculations.

Keywords: radon, tobacco smoke, vdW-DF, van der Waals, DFT.

Acknowledgements

I would like to give a word of thanks to my supervisor Per Hyldgaard who has been a constant source of inspiration during the work on this thesis. I would also like to thank Eskil Varenius with whom I've been working closely during a large portion of the time.

Also thanks to all the other people at the BioNano Physics Laboratory and Quantum Device Physics Laboratory who have helped providing a warm and inspiring environment.

An extra word of thanks to Marcin Dulak at Copenhagen University who kindly provided me with his experimental PAW setups.

Göteborg, June 2011
Magnus Sandén

Contents

Abstract . . . iii
Acknowledgements . . . v

1 Introduction **1**
1.1 Radon . . . 1
1.2 Tobacco smoke and radon . . . 3
1.3 Van der Waals interaction . . . 4
1.4 Purpose . . . 5
1.5 Overview of thesis . . . 6

2 Theory **7**
2.1 Density functional theory . . . 7
2.2 Projector augmented wave method . . . 14
2.3 Forces and structure relaxation . . . 16

3 Calculation approach **17**
3.1 Selection of molecules . . . 17
3.2 Software packages . . . 17
3.3 Explanation and choices of parameters . . . 18
3.4 Test of noble gas setups . . . 19
3.5 Adsorption on molecules . . . 20
3.6 Adsorption on PAH molecules . . . 22
3.7 Radon on nitrosamines and nicotine . . . 23

4 Results **26**
4.1 Test of noble gas setups . . . 26
4.2 Adsorption sites on benzo[a]pyrene . . . 27
4.3 Summary of adsorption energies and distances . . . 27

5 Discussion and outlook **30**
5.1 Size of molecules and atoms . . . 30
5.2 vdW-DF . . . 31
5.3 Outlook . . . 31

Bibliography **33**

Chapter 1

Introduction

It is an exciting time right now when the advances in numerical physics and computer technology add up to the point where we can start to do quantum mechanical simulations of biological systems. This will inevitably lead to a greater knowledge of the immense complexity of the human body, and will also lead to better understanding of some of the ailments that can afflict us.

Currently about 3000 people die from lung cancer every day [2]. Fortunately we know pretty well what the most common causes for lung cancer are. 90% of all lung cancer cases are due to tobacco usage [3]. The second largest cause for lung cancer is radon. Among non-smokers, radon is the largest cause for lung cancer.

This work aims at providing better knowledge about these two causes for lung cancer. More specifically I have been trying to find an explanation for why smokers are affected more by radon than non-smokers. This has been done through first principle electronic structure calculations of the interactions between radon and tobacco-smoke particles.

1.1 Radon

Radon (^{222}Rn) is a radioactive noble gas that results from the decay of radium (^{226}Ra). It is part of the decay chain of uranium (^{238}U) (sometimes called the radium decay chain) and is thus naturally occurring wherever uranium can be found. At room temperature it is a colourless, odourless gas [4]. Radon is a carcinogen [5], which doesn't come as a surprise knowing that it is radioactive.

When radium decays into radon it emanates from the rock and goes off into the air. Higher concentrations of radon are gathered in enclosed spaces such as mines and houses. Radon mainly enters houses from the soil under the house [4], and to a lesser degree through building materials and water [6]. Being a noble gas radon it is somewhat difficult to stop (though not impossible as we will soon find out). The usual method is instead to employ extra ventilation.

Radon decays with a half-life of about four days. Its daughters (decay products) on the other hand are much shorter lived with half-lives of between a few milliseconds up to about half an hour. The decay chain comes to a pause with lead (^{210}Pb) which, with a half-life of 22.3 years, can almost be considered stable. This lead isotope can be accumulated in the body to significantly mea-

Figure 1.1: Radon has not always been considered dangerous. This commercial poster for a Swedish brand of spring water claims that the water is strongly radioactive and thus very healthy and even recommended by doctors.

surable levels [7]. The decay finally stops with another lead isotope, namely ^{206}Pb, which is stable.

Detection of radon can be done by setting up boxes with activated carbon in the house. The radon atoms adsorb on the very large surface area of the activated carbon and the radioactivity of the coal can be used to gauge the concentration of radon in the indoor air. The fact that the radon adsorbs so well on the activated carbon leads us to think that it might also adsorb on other organic compounds, such as the lung interior and, in particular, the organic molecules in tobacco smoke or other types of smoke.

People exposed to radon have an increased risk of lung cancer [5]. The reason for this is that the radon and its daughter nuclei follow the air into the lung where they can decay and deposit their radiation [8]. Radon and several of its daughters give off α-radiation as they decay. This radiation can severely damage the lungs and if the DNA is injured, this might lead to cancer. It is also possible that the heavy metal radon daughters (such as lead) can contribute to the overall increase in lung cancer risk through chemical impact. Inorganic lead has been classified as "probably carcinogenic to humans" by the International Agency for Research on Cancer [9]. Apart from this lead is also known to be neurotoxic to humans [10].

The daughters of radon can also enter the body by an alternative means, aerosol particles. Although metal atoms readily bind to surfaces (such as the floor, walls and ceiling of a room), some of them will remain mobile in the air if there are enough small dust particles in the air. In fact, most (typically about

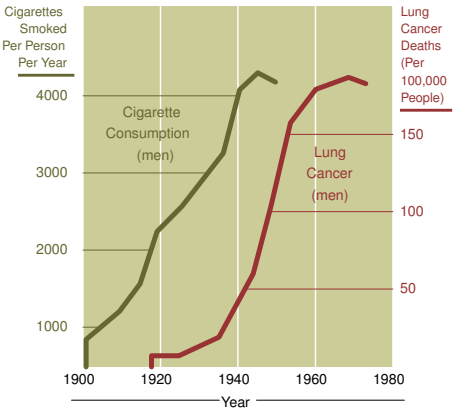

Figure 1.2: Smoking and lung cancer deaths among US males between 1900 and 1980. A 20-year lag can be seen between the increase in smoking and the increase in lung cancer deaths. [Picture from Wikipedia. The picture is considered to be in the public domain.]

90%) of the daughter nuclei of radon are attached to some aerosols dust particles [7]. Because of this, they stay airborne longer and have a higher likelihood of being breathed in.

1.2 Tobacco smoke and radon

Chemical analysis of tobacco smoke is not easy. The curing, filtering and all the additives in commercial cigarettes differ from one brand to another. All in all tobacco smoke consists of several thousand chemical compounds [11]. Several of these are potent carcinogens. Some important constituents of tobacco smoke are polycyclic aromatic hydrocarbons (PAH) and these are in fact also found in other types of smoke. Other constituents are more unique to tobacco smoke, such as nicotine and tobacco specific nitrosamines. (Pictures of these molecules can be seen in figures 3.3 and 3.6.)

In 1950 Doll and Hill published an article [12] which clearly proved the connection between tobacco smoking and lung cancer. In 1986 the International Agency for Research on Cancer published a monograph [13] that concludes that tobacco smoking is carcinogenic to humans. By the year 2000 smoking had either peaked or declined in all developed countries, but it continued to rise in the developing world. Still today cigarette smoking is the leading cause of lung cancer [3]. The World Health Organisation estimates that every year as many as 5 million people die from tobacco use [14].

As it turns out, radon affects smokers more than non-smokers [15][8][7]. This is after taking into account the already heightened risk for lung cancer among smokers. As far as I know the reason for this connection has not been fully quantified. Finding the reason behind the connection between radon and tobacco smoking is important, not only for smokers but also for other people exposed to PAH molecules. This includes passive smokers and people who use an open fireplace in a room with radon.

A few possible scenarios for introduction of radon and its daughters into the lungs spring to mind. Perhaps the radon atoms adsorbs onto some molecule in the smoke and follows the smoke into the lungs. Perhaps the tar in the smokers lungs makes the radon more likely to stay in the lungs. In any case, if radon or any of its daughters end up in the lungs, there will be damage from α-particles and/or from an accumulation of lead atoms after the decay chain has reached its end.

It is not immediately clear which of these scenarios that is most likely and therefore the most serious problem when mixing radon with smoking. It is certainly clear that ^{210}Pb has a longer life time and therefore should have a higher probability for sticking in our lung than radon. Since radon is a noble gas, in a naive analysis one would expect it to have a vanishing probability of sticking to the smoke particles. Nevertheless the long lived lead daughters of radon have lower radioactivity, and there is no consensus that one can ignore the danger from the α-particle emission directly from radon.

In this thesis we seek to refine the understanding of radon's inertness, arguing that smoke may provide a way for direct introduction of the very radioactive radon into the lungs. We can quantify the likelihood of having radon irreversibly stick to smoke particles, which themselves have a raised likelihood of sticking in lungs (as smokers experience). Smoke thus provides a way to cause the damaging local radiation as well as a subsequent inclusion of toxic lead atoms. We document that a picture of radon as inert is an oversimplification. Radon will most certainly bind with a sufficient strength to smoke particles. The ramifications are potentially important for how we think about radon mitigation measures.

1.3 Van der Waals interaction

We next turn our attention to the nature of the interaction that lets radon atoms bind to the smoke particles. The van der Waals (vdW) force is a long range force between any two atoms or molecules. Between two neutral atoms or molecules without permanent dipole momenta its the only existing interaction (except for Pauli exclusion). It is a part of the electrodynamic interaction of the atoms but is in some cases separated out as a distinct feature.

There is some inconsistency in the literature about how to use the word van der Waals forces. With van der Waals forces I will henceforth mean exclusively the London dispersion interaction between atoms and molecules without permanent dipole momenta. These effects are named after Fritz London who first described them.

Van der Waals forces are ubiquitous in nature and understanding them is therefore important. A few examples of systems where the van der Waals forces add up to give macroscopic effects can be seen in figure 1.3.

The van der Waals force is often described as a result of an instantaneous dipole in one atom inducing a dipole in the other atoms. These dipoles then interact with an energy that goes as $E(R) \propto R^{-6}$ at asymptotic separation R. This simple picture is not unproblematic though. It has some difficulties explaining the presence of the van der Waals interaction at low temperatures where the electron density should be constant in time [17].

I will instead employ a view of the van der Waals interaction as a result

Figure 1.3: Examples of van der Waals bound systems. Left: the layers in a graphite crystal are bound by van der Waals forces. The layers can peel off easily which is the reason we can write with graphite pencils. Right: the feet of the gecko lizard are covered with millions of tiny "hairs" that add up to big surface area which gives a high van der Waals attraction and allows the gecko to climb on even very smooth surfaces such as polished glass [16]. [Left image with permission by R. Weller/Cochise College. Right image from Wikipedia, CC-BY-SA and GFDL.]

of quantum mechanical oscillations under a constant electron density. In this picture the energy dip can be explained with two coupled harmonic oscillators (see for example Kittel [18], chapter 3). This system can then drop its energy by letting the oscillations line up, which, to first order in R^{-1}, gives an energy drop

$$E(R) = -\frac{C_6}{R^6}\,, \tag{1.1}$$

where R is the separation between the oscillators and C_6 is a constant. This gives a good description of the energy curve at asymptotic separations, but it is still not enough to give a physically sound description of the origin of the van der Waals force.

Assuming that the atomic cores can be seen as classical particles, the van der Waals forces acting on them must be due to some static charge redistribution near the atomic core [19]. This is easily understood since the atomic nuclei only feel the electrostatic Coulomb force from the electron density and should thus be impervious to any quantum mechanical oscillations. So in order to get a force on the nucleus there must also be some charge redistribution stemming from these oscillations. This static redistribution was recently quantified for an argon dimer using non-empirical density functional theory calculations [20].

1.4 Purpose

In this thesis I wish to investigate if there is any binding of radon atoms to molecules of tobacco smoke and, if so, how strong these bindings are. I will do this through first-principle electronic structure calculations. It will turn out that

the picture of radon as an unstoppable inert gas with no tendency to interact with other molecules is a big simplification.

The second purpose of this thesis is to evaluate and compare the two different versions of the van der Waals density functional used to model van der Waals interactions in density functional theory.

1.5 Overview of thesis

This thesis is structured as follows. In chapter 2 I will go through the basics of density functional theory. In chapter 3 I will describe how the calculations have been performed and in chapter 4 I will present my results. Chapter 5 is where I present my conclusions and give some outlook of what the future might hold.

Chapter 2

Theory

The Schrödinger equation provides us with a description of how non-relativistic electrons behave. It's solutions dictate most of how atoms and molecules interact with each other. It can be solved analytically for some simple systems with only one electron, such as the isolated hydrogen atom or the harmonic oscillator. For most other systems we have to resort to solving it numerically.

For one electron it is still not very difficult. However, nature mostly consists of systems of more than one electron, and that's where things get tricky. When the number of particles increase the computational cost of naive computational schemes soon becomes unfeasible. We have to do something completely different.

One widely used method is *density functional theory* (DFT), which is popular for several reasons. It can provide good results for a wide array of atomic systems with a reasonable computational time. DFT is also non-empirical, which promises a higher degree of transferability. That is, it should in principle be applicable to any electronic structure problem, and when there are few experiments (as in the radon case), non-empirical methods are the only options.

A shortcoming of density functional theory has, until recently, been its inability to model the long range van der Waals interaction. The development and improvements of the van der Waals density functional during the last decade make non-empirical calculations of van der Waals systems possible in the DFT framework.

I will first go through the fundamental theory underpinning DFT. After that I will talk about how many-body effects and van der Waals interactions are modelled in DFT. The next part of this chapter will be about the PAW formalism. Lastly I will briefly mention how equilibrium *atomic* structures can also be calculated using DFT.

All equations in this chapter are in Hartree atomic units, which are chosen so that

$$\hbar = e = m_e = 4\pi\epsilon_0 = 1\,.$$

2.1 Density functional theory

DFT is a popular tool for determining the electronic structure of different systems. It was first developed in the 1960's and with further developments throughout the years it has become increasingly accurate, versatile and fast. A

recent key progress in density functional theory is the van der Waals density functional, which has helped make this investigation possible.

Density functional theory (DFT) is a method for solving the many-particle Schrödinger equation in an efficient way. It does this by providing a way to transition from one many-particle Schrödinger equation to many one-particle equations. The interaction of the electrons is contained inside an effective potential.

In DFT we will always make use of the Born-Oppenheimer approximation, in which the kinetic energy of the nuclei is neglected. This simplifies the Schrödinger equation as only the electrons need to be treated quantum mechanically.

A key idea behind DFT is that instead of using the wave functions as fundamental variables we can use the electron density. This simplifies matters a lot. To be able to do this transition we need something that guarantees that we don't lose any information, which is where the theorems of Hohenberg and Kohn enter.

2.1.1 Hohenberg-Kohn theorems

These two theorems provide the theoretical foundation for all of density functional theory. Their surprisingly simple proofs were provided in 1964 by Hohenberg and Kohn [21]. Other, more general, proofs of these theorems have since been constructed. For proofs and a more detailed review of these theorems see for example Martin [22], chapter six.

The first theorem says that the ground state electron density of a system of electrons uniquely determines the external potential (up to an additive constant) that these electrons reside in. This also means that with only the ground state density one can reconstruct the Hamiltonian of the system, and thus one would in principle have access to all the properties of the system.

The second theorem states that there exists a universal functional $F[n(r)]$ of the density $n(r)$ such that

$$E[n(r)] = F[n(r)] + \int V_{\text{ext}}(r)n(r)\mathrm{d}r \tag{2.1}$$

has its minimum for the ground state density. In this functional the external potential $V_{\text{ext}}(r)$ can for example be the Coulomb potential from the nuclei. The minimum value of the functional is then the total energy of the system.

Together these theorems state that, in theory, it is possible to exactly determine the ground state density by minimising the functional $E[n(r)]$. Then, in theory, one can exactly determine all properties of the system in question.

Problem is, we don't know what the universal functional $F[n(r)]$ looks like. So by themselves, the theorems of Hohenberg and Kohn don't provide us with any clues as to how to actually calculate anything. It was one year later, in 1965, that Kohn and Sham suggested a way of putting these theorems to practical use.

2.1.2 The Kohn-Sham approach

The main idea in the Kohn-Sham approach [23] is to rewrite the problem in terms of an auxiliary system. The particles of this auxiliary that are like electrons in all aspects, except that they interact exclusively with the overall electron density through a term $E_H[n]$. This auxiliary system must for example have the same number of electrons and the same density as the original problem.

The energy functional for this auxiliary system is simple to write in terms of the density:

$$E_{\text{aux}}[n] = T_s[n] + E_H[n] + \int V_{ext}(r)n(r)\mathrm{d}r\,,$$

where

$$T_s = \sum_i \langle\psi_i| - \frac{1}{2}\nabla^2|\psi_i\rangle$$

is the kinetic energy for these auxiliary particles and

$$E_H[n] = \int \frac{n(r)n(r')}{|r-r'|}\mathrm{d}r\mathrm{d}r'$$

is the energy due to the Coulomb interaction with the density.

That is all well and good, but we want this new auxiliary system to actually say something about the original problem. In particular we want it to have the same total energy. Formally, this is easily achieved by adding a term $E_{xc}[n]$ to the energy functional.

$$E[n] = T_s[n] + E_H[n] + \int V_{ext}(r)n(r)\mathrm{d}r + E_{xc}[n] \tag{2.2}$$

The term $E_{xc}[n]$ corresponds to the contribution from many-body effects and is called the *exchange correlation energy*. It should contain whatever is needed to make this total energy functional the same as in the original fully interacting problem. Comparing equations 2.1 and 2.2 we can see that E_{xc} can be written in terms of $F[n]$.

$$E_{xc}[n] = F[n] - T_s[n] - E_H[n] \tag{2.3}$$

Since all the term on the right hand side in 2.3 are universal, E_{xc} must also be a universal functional.

We still don't know what E_{xc} looks like though. The reason to write the total energy functional as in equation 2.2 is that all terms except E_{xc} can written down exactly, and E_{xc} is usually the smallest contribution to the total energy. Accurate approximations for E_{xc} provides the very core of the immense success that DFT has experienced over the last few decades. I will more talk about such approximations of E_{xc} in section 2.1.5.

According to Hohenberg and Kohn, we want to minimise the functional $E[n]$ in order to find the ground state of the system. We will try to find the minimum using the variational principle. We can do this by varying n directly, but in the Kohn and Sham approach we vary with respect to the auxiliary wave functions $\psi_i(r)$ and $\psi_i^\star(r)$ instead.

We require that these auxiliary wave functions must be normalised. We can add this constraint to the minimisation problem through Lagrange multipliers.

So instead of minimising 2.2 directly we want to minimise the functional

$$E[n] - \sum_i \epsilon_i \left(\int \psi_i^\star(r)\psi_i(r)\mathrm{d}r - 1 \right) ,$$

by varying with respect to $\psi_k^\star$ we can see when this is achieved.

$$0 = \delta E[n] - \epsilon_k \int \delta\psi_k^\star \psi_k \mathrm{d}r = \int \mathrm{d}r \left(\frac{\delta E[n]}{\delta\psi_k^\star(r)} - \epsilon_k \psi_k \right) \delta\psi_k^\star(r)$$

This should be true for any variation $\delta\psi_k^\star$ which means that the rest of the integrand must be zero. That is

$$\frac{\delta E[n]}{\delta\psi_k^\star(r)} = \epsilon_k \psi_k \, .$$

The functional derivative of $E[n]$ consists of two parts. The derivative of the kinetic energy term $T_s[n]$ becomes:

$$\frac{\delta T_s[n]}{\delta\psi_k^\star(r)} = -\frac{1}{2}\nabla^2\psi_k(r)$$

and all the other terms can be collected in an effective potential:

$$\left(\frac{\delta E_H[n]}{\delta n(r)} + V_{\mathrm{ext}}(r) + \frac{\delta E_{xc}[n]}{\delta n(r)} \right) \frac{\delta n(r)}{\delta\psi_k^\star(r)} = V_{\mathrm{eff}}(r)\psi_k(r) \, , \tag{2.4}$$

where I used the relation

$$\frac{\delta n(r)}{\delta\psi_k^\star(r)} = \psi_k(r)$$

and the definition

$$V_{\mathrm{eff}}(r) = \frac{\delta E_H[n]}{\delta n(r)} + V_{\mathrm{ext}}(r) + \frac{\delta E_{xc}[n]}{\delta n(r)} \, .$$

Putting it all together, we arrive at the Kohn-Sham equation

$$\left(-\frac{1}{2}\nabla^2 + V_{\mathrm{eff}} \right) \psi_i = \epsilon_i \psi_i \, . \tag{2.5}$$

At first glance this looks like a time-independent Schrödinger equation, but once you look closer you realise that V_{eff} depends on all the orbitals $\psi_i(r)$. Kohn and Sham suggested that one should solve the equation iteratively.

The Hohenberg-Kohn theorems imply that we can solve the many-particle Schrödinger equation without having to fiddle with the complicated wave functions. In the Kohn-Sham equation 2.5 there are still wave functions there, but this time they are single-particle wave functions, which means that they are much more simple to deal with. Indeed this is the one of the best ways known to obtain a good approximation for the density of the fully interacting system.

2.1.3 The self-consistency loop

The iterative process of solving the Kohn-Sham equations 2.5 is often called the self-consistency loop. It goes as follows.

1. Create a roughly accurate electron density for initial guess.
2. Calculate what effective potential V_{eff} that this density corresponds to.
3. Solve the Kohn-Sham equations with that potential.
4. Calculate a new electron density by mixing the old density with the new density from the solutions in step 3.
5. Go back to step 2.

This procedure is iterated until converged. That is until the density, wave functions and energy all change less than some predefined limits.

2.1.4 Remaining questions

It should be noted at this point that there are a few things that remain unclear. Will this procedure converge? Is there always an auxiliary system such that $\sum_i |\psi_i(r)|^2 = n(r)$? What's the expression for E_{xc}? I have left these questions out of the preceding text on purpose as their answers are not easy.

The convergence of the Kohn-Sham procedure is not a trivial issue, as it depends on initial guess and mixing scheme as well as numerical noise during the calculations. There are several different mixing schemes and methods of creating an initial guess. For the purpose of this thesis it is sufficient to note that I have gotten all of my calculations to converge. For a more in-depth discussion of convergence and mixing schemes, see Martin [22], chapter 9.

Kohn and Sham had as an implicit ansatz that for a system of electrons, an auxiliary system (such as in section 2.1.2) with the same ground state density can be created. This ansatz has not been rigorously proven for real systems of interest [22]. In the same spirit as Kohn and Sham we shall instead take it in good faith that it is possible for all the systems that I will be working with.

The last big question mark is the exchange correlation functional $E_{xc}[n]$, but that needs a longer, separate discussion.

2.1.5 Exchange correlation functional

So far everything we have done has been formally exact. Unfortunately we do not know the exact functional $F[n]$ from Hohenberg and Kohn's theorem, and so we do not know the exact form for the exchange correlation functional in the Kohn-Sham approach. This is where we start to approximate $E_{xc}[n]$.

The exchange correlation energy is the extra energy that the electrons have because of their mutual interactions. As the name suggests, it can be split into two parts which can be approximated separately: the exchange energy and the correlation energy.

Since electrons are fermions they have to obey the Pauli exclusion principle. It might increase the electrons energy to do so. This energy increase is called the exchange energy.

The correlation energy is the extra energy of the electrons because of their mutual electrodynamic Coulomb interaction. All the difficult many-body effects are included in this small correction term.

There is a wealth of different functionals that all try to approximate the exchange correlation energy in different ways. As it is one of the focal points for the theoretical development of the DFT method, new exchange correlation functionals pop up at a steady rate.

Local density approximation

The simplest of all the exchange-correlation functionals and also the one used by Kohn and Sham in their original paper is called *local density approximation* (LDA). It approximates the electron density to be constant in each point. The LDA functional is thus accurate for slowly varying electron densities. It gives surprisingly good results for many systems considering how crude of an approximation it is.

We can split the LDA functional into exchange and correlation parts.

$$E_{xc}^{\mathrm{LDA}} = \int \mathrm{d}r n(r)(\epsilon_x(n(r)) + \epsilon_c(n(r)))$$

Note that each $\epsilon(n(r))$ is only a function of the density at one point. The exchange energy density $\epsilon_x(n(r))$ of a homogeneous electron gas can be calculated exactly [23], whereas the correlation energy density $\epsilon_c(n(r))$ has been accurately computed through quantum Monte Carlo simulations. For further information about the local density approximation see Martin [22], chapter 8 and appendix B.

Generalised gradient approximation

In order to be able to accurately describe more rapidly varying electron densities one can also let the functional depend on the gradient of the electron density. A straight forward way of doing this is called the *gradient expansion approximation* (GEA). It was suggested by Kohn and Sham in their paper [23]. Unfortunately this method breaks down when the the gradients become too big, and in fact, in real materials the gradients are bigger than what GEA can handle.

A better way of doing this is the *generalised gradient approximation* (GGA), which gives consistently better results than LDA. The difference between GEA and GGA is in the way that the functional handles large gradients.

GGA lets the functional be aware of not only the electron density at one point, but also of an infinitesimal surrounding to that one point. Even though this might not sound like a huge improvement over LDA the results are much better.

Several of these GGA functionals have been developed over the years. One of the most commonly used GGA functionals was constructed by Perdew, Burke and Ernzerhof in 1996 [24][25] and is called *PBE*. An updated version of the PBE functional is the *revPBE* [26] functional, which I have used extensively in this report.

For a more in depth discussion of GGA-functionals see Martin [22], chapter 8 and appendix B.

Van der Waals density functional

A common feature of most exchange correlation functionals is, however, that they lack a good description of the van der Waals forces (illustrated in figure 3.2). This is not true for all functionals though. The aptly named *van der Waals density functional* (or vdW-DF for short) was developed to include also these weak long range forces [27][28][20]. It consists of GGA exchange, LDA correlation and a truly non-local correlation part.

$$E_{xc}^{\mathrm{vdW}}[n] = E_x^{\mathrm{GGA}}[n] + E_c^{\mathrm{LDA}}[n] + E_c^{\mathrm{nl}}[n]$$

The non-local part of the correlation energy is evaluated as a six dimensional integral:

$$E_c^{\mathrm{nl}}[n] = \int\int \mathrm{d}r\mathrm{d}r' n(r)\phi(r,r')n(r')\,, \tag{2.6}$$

where the kernel $\phi(r,r')$ describes the correlation of electronic oscillations (plasmons) at positions r and r' integrated over all plasmon frequencies. In the asymptotic limit the functional gets the well-known R^{-6} behaviour mentioned in section 1.3.

A derivation of the kernel is far beyond the scope of this thesis. A description of how the kernel can be evaluated is presented in Thonhauser et al. [20], appendix A, and a thorough derivation of the kernel expression can be found in Berland's licensiate thesis [17], chapter 3 and appendix A.

There are also a few other methods of describing the van der Waals interactions within the DFT framework. To my knowledge vdW-DF is almost unique in that it is also derived from first principle. As such it promises to be applicable to a wide range of systems and to give some insight into the underlying physical phenomena. For a recent review of some of these different methods see Grimme [29].

A more recent version of vdW-DF was proposed in 2010 [30] and is called vdW-DF2. This new version aims at providing more accurate binding distances and energies in the van der Waals dominated region. Since it is still a very new functional it is interesting to evaluate its performance compared to the original vdW-DF.

2.1.6 Non self-consistent calculations

After the ground state density has been found by minimising the energy functional, the ground state energy is calculated. This can in principle be done by inserting the density and the Kohn Sham orbitals into the expression for the energy functional 2.2. If the same exchange correlation functional was used during the self consistency loop as was used to calculate the energy, it is called a *self-consistent* calculation.

One can also calculate the electron density using one approximation for the exchange correlation functional (e.g. revPBE), and then plug that density into the energy expression with *another* exchange correlation functional (e.g. vdW-DF). It is then called a *non self-consistent* calculation and gives good results if the ground state density is approximately the same for both of these functionals.

The reason to do this is that the evaluation of the six dimensional integral in the vdW-DF functional makes it more numerically demanding than LDA or

GGA functionals. So if the self-consistency loop can be done with GGA instead of vdW-DF there is a clear speed up. It turns out that in most cases this is a good approximations, at least at binding separation and at larger separations [20].

The downside of doing non self-consistent calculations is that the charge redistribution due to the van der Waals interactions is completely ignored. Because of this the forces and relaxations of the nuclei (see section 2.3) in simple implementations of forces will also not include the van der Waals interactions. When the forces are not needed non self-consistent calculations are a useful technique for speeding up the calculations.

2.2 Projector augmented wave method

Even after the great simplification provided by the Kohn-Sham scheme the equations remain somewhat difficult to solve numerically. However since we always solve them for systems of atoms, we can specialise the algorithm to be efficient for such systems.

The main problem with such systems is that the solutions to the Kohn-Sham equations behave drastically different in different regions in space. Far away for the atomic core the valence wave functions will be smooth, but they will change a lot depending on the environment of the atom. From this we could guess that a simple uniform grid would be suitable. Near the atom cores the valence electrons wave functions will oscillate rapidly in order to be orthogonal to the wave functions of the inner (core) electrons. Unfortunately, this means that a simple uniform grid would have to be too fine to be numerically feasible. A better approach is to divide space into different regions and treat them differently. This is what is done in the *projector augmented wave* (PAW) method that I have been using.

The projector augmented wave method is a numerically efficient way of solving the Kohn-Sham equation. It was introduced in 1994 by Blöchl [31] and can be seen as a generalisation of several earlier methods.

It divides space into atomic regions close to the atoms and an interstitial region. The strategy is to be able to represent the true wave function as a combination of a smooth pseudo wave function present in all of space and some correction parts localised around each atom. The smooth pseudo wave function can easily be represented using a sparse uniform grid and the atom centred parts can easily be represented using for example atomic orbitals on finer radial grids.

Another division is made in the PAW-method, namely between core electrons and valence electrons. The core electrons are not affected much by the environment surrounding the atom. Thus their wave functions are calculated once and for all for each atomic species and are not allowed to change during the calculation. This is known as the *frozen core approximation* and, although not crucial for the PAW-method [31], it is generally used. The valence electrons are affected a lot by the surroundings and are treated in more detail next.

2.2.1 Decomposing the wave function

At the heart of the PAW method, there is a transformation of the wave function. This transformation allows us to go back and forth between the true *all-electron*

wave function $|\Psi_i\rangle$ and a smooth *pseudo* wave function $|\tilde{\Psi}_i\rangle$. Since the all-electron wave function is already smooth in the region between the atoms we can require that the smooth wave function should be the same as the true wave function outside a sphere centred around each atom.

The transformation can then be written on a quite simple form:

$$|\Psi_i\rangle = |\tilde{\Psi}_i\rangle + |\Phi_i\rangle - |\tilde{\Phi}_i\rangle \ , \tag{2.7}$$

where the first term is smooth everywhere and can be represented on a sparse uniform grid in all space. The last two terms correspond to corrections within the atomic regions. $|\Phi_i\rangle$ should be identical to the true all-electron wave function $|\Psi_i\rangle$ inside the atomic regions, whereas $|\tilde{\Phi}_i\rangle$ is identical to the pseudo wave function $|\tilde{\Psi}_i\rangle$ inside the atomic regions. These two terms need a finer grid but are on the other hand localised to inside the atomic regions.

This way of rewriting the wave function is the basic idea behind the PAW method. It is illustrated in figure 2.1.

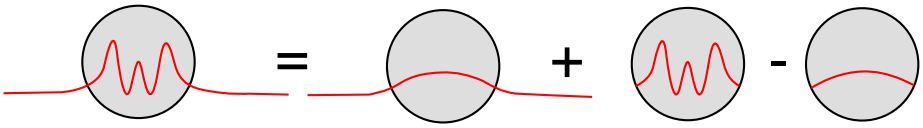

Figure 2.1: The different parts of a valence wave function in the PAW method. An illustration of the different terms in equation 2.7.

We want to be sure that the valence states are orthogonal to the core states throughout the calculations. We can achieve this by introducing an expansion of the last two terms in 2.7. The basis of the expansion should be the set of atomic orbitals for the free atom. The core states will occupy some of these orbitals and the basis set for the valence states can be restricted to all orbitals not occupied by core states. The coefficients in the expansion can be calculated using so called *projector functions*. For more information on these projector functions and how they are chosen I refer to Blöchl [31].

We have now arrived at a position where each of the terms in equation 2.7 can be represented in some numerically efficient way, but to add all the terms together would still require the same numerically inefficient fine grid as before. Instead we want to be able to do all the calculations without ever calculating the true all-electron wave functions. To be able to do this we need to rewrite all the things that we use during the self-consistency cycle in terms of $|\tilde{\Psi}_i\rangle$, $|\Phi_i\rangle$ and $|\tilde{\Phi}_i\rangle$. The Kohn-Sham equations, the energy operator, the density operator all need to be rewritten. This is possible to do by applying the same transformation as was used on the wave functions. Expressions for these things can be found in [31] and [32].

2.2.2 Preparing a PAW calculation

Before you can perform an actual calculation in PAW you have make some preparations. These are needed for each atomic species used in the calculations.

The steps that are needed are:

- Decide which electrons are to be considered valence electrons.
- Define an augmentation region.
- Solve the single atom problem in order to get the core states.
- Orthogonalise the valence basis set with respect to the core states.
- Create some projectors.

All these steps are done once and for all for each atomic species.

2.3 Forces and structure relaxation

When the electron density is known, one can calculate the forces acting on the nuclei. The force on the nucleus i at position R_i can be calculated from

$$\mathbf{F}_i = -\frac{\partial E}{\partial \mathbf{R}_i} = -\frac{\partial}{\partial \mathbf{R}_i} \langle \Psi | H | \Psi \rangle \ ,$$

where $|\Psi\rangle$ is the normalised many-body wave function. Using first-order perturbation theory we can write this as

$$\mathbf{F}_i = -\langle \Psi | \frac{\partial H}{\partial \mathbf{R}_i} | \Psi \rangle - \langle \frac{\partial \Psi}{\partial \mathbf{R}_i} | H | \Psi \rangle - \langle \Psi | H | \frac{\partial \Psi}{\partial \mathbf{R}_i} \rangle - \frac{\partial E_{II}}{\partial \mathbf{R}_i} \ , \tag{2.8}$$

where I have introduced a new term to the total energy, namely E_{II}. This term corresponds to the energy of the interaction between the nuclei and is simply a classical Coulomb interaction. The second and third terms of 2.8 vanish because at the exact ground state the wave function corresponds to an energy extremal and thus any infinitesimal change in the wave function will not affect the total energy. This leaves us with

$$\mathbf{F}_i = -\langle \Psi | \frac{\partial H}{\partial \mathbf{R}_i} | \Psi \rangle - \frac{\partial E_{II}}{\partial \mathbf{R}_i} \ .$$

The only term in the hamiltonian that explicitly depends on the positions of the nuclei is V_{ext}. The expression can thus be further simplified to

$$\mathbf{F}_i = -\int \mathrm{d}^3 r \, n(r) \frac{\partial V_{\text{ext}}}{\partial \mathbf{R}_i} - \frac{\partial E_{II}}{\partial \mathbf{R}_i} \ .$$

For more details on this theorem and some comments on its history see Martin [22], chapter 3.

Knowing the forces that act upon the nuclei opens up a range of interesting possibilities. It is possible to minimise the forces through standard optimisation routines, in each step moving the nuclei according to these forces and performing a new DFT calculation with the atoms at these new positions. This optimisation is then performed until the calculated forces are less than some predefined limit. It is possible to use both local optimisation algorithms and global optimisation algorithms to find the energetically favourable atomic positions.

It should be noted that in each DFT calculation it is still assumed that the nuclei are fixed according to the Born-Oppenheimer approximation. The atoms are only moved *between* each DFT calculation.

Chapter 3

Calculation approach

In this chapter I will discuss some of the choices that I have made for this thesis. We first turn to the question of choosing which molecules to use. After that I will discuss my calculation scheme, the DFT-implementation I have used, as well as the computational parameters.

3.1 Selection of molecules

Tobacco smoke consists of thousands of different chemical compounds [11]. Things like curing, filters, smoking conditions etc, all affect the composition of the smoke. Unfortunately it has not been possible to make an exhaustive investigation of all the compounds.

I have instead chosen a number of interesting molecules and investigated the possible adsorption on those. The molecules that I chose are well documented to exist in tobacco smoke.

I chose some polycyclic aromatic hydrocarbons (PAH) both because we suspected adsorption on those and because they can be found in many other types of smoke. Benzene, benzo[e]pyrene, benzo[a]pyrene and coronene are all examples of PAH molecules that have been found in tobacco smoke [11].

The other molecules I chose to investigate where two tobacco specific nitrosamines called NNK (4-(methylnitrosamino)-1-(3-pyridyl)-1-butanone) and NNN (N-Nitrosonornicotine) and finally nicotine. All of these can be found in tobacco smoke [11].

Finally, I have done calculations on graphene. Although no infinite sheets of graphene are present in smoke, it is interesting as part of a trend study where I investigared how the size of the molecule affects the strength of the binding.

3.2 Software packages

All the calculations presented in this thesis have been performed using the software package GPAW [33][34]. GPAW stands for *Grid-based Projector Augmented Wave* and is an implementation of the PAW formalism discussed in section 2.2. It is integrated with the *Atomic Simulation Environment* [35] (ASE) which is a python environment that enables easy access to several different calculators such as GPAW.

Since the currently stable version of GPAW didn't include a way to choose vdW-DF2 as exchange correlation functional I used a development version of GPAW, namely revision 7883. When it comes to ASE I used the default version on the Beda cluster, which was version 3.4.1.1861.

GPAW is responsible for doing the actual DFT calculations; it performs the self-consistency loop and calculates the energy and forces. ASE takes care everything else, such as setting up the atoms and moving the atoms during an atomic structure relaxation. Several optimisation algorithms are available in ASE, but for all the relaxations that I have performed I have used BFGS, which is a Quasi-Newton algorithm.

3.3 Explanation and choices of parameters

Density functional theory could in principle be parameter-free, but an actual implementation is far from it. I will try to briefly explain some of the parameters and settings in GPAW.

The first and most obvious setting that one has to do is to choose the *exchange correlation functional*. In my calculations of noble gases the van der Waals forces play a dominant role, and I have thus chosen to use the vdW-DF functional. I have also found it interesting to compare it to the newer version vdW-DF2. GPAW includes implementations of both of the functionals vdW-DF and vdW-DF2, as well as LDA and several flavours of GGA.

In all non self-consistent calculations, except for the bulk calculations, the self consistent density was calculated using revPBE and inserted into vdW-DF and vdW-DF2. In the noble gas bulk calculations (see section 3.4.1) the self consistent density was calculated using PBE.

Another important setting to consider is the size of the *unit cell* and its *boundary conditions*. In the case of the bulk calculations I used periodic boundary conditions in all directions. The cell size is then simply the nearest neighbour distance in each direction. In the other calculations I used zero boundary conditions in all directions and the cell sizes were chosen so that there should be enough vacuum around each of the atoms. The cell sizes used can be found in the sections corresponding to the different calculations.

In the PAW method one uses a uniform grid over all of space for the first term in equation 2.7. The *grid spacing* of this grid can be set in GPAW and defaults to 0.2 Å. In the bulk calculations the grid spacing was set to 0.07 Å, whereas in the other calculations I used the default value.

GPAW gives the user a lot of control over the *mixer* used to mix the new density into the old density. One can control how much of the new density is used and how much of the old density, as well as how many of the last few densities should be used. Changing these parameters can be very helpful in order to get the calculations to converge.

Another setting that I have fiddled with on my quest for convergence is the *eigensolver*. A few different algorithms for solving the eigenvalue problem in step 3 in section 2.1.3 are available. According to the GPAW website, the default eigensolver called *rmm-diis* trades convergence properties for speed [36]. In some cases I have instead been using the eigensolver called *conjugate gradient*.

Evaluation of many quantities in DFT, such as energy and density, appear as integrals over k-space (Fourier space). Numerical evaluation of such integrals

require that they are discretised into a sum. In GPAW the user is of course free to choose the *k-point sampling*. There has been much studying in how to choose these points in an efficient way (see Martin [22], chapter 4 for a summary).

For the non-periodic systems only one point of the Brillouin zone was sampled, namely the central point (the Γ-point). In the bulk calculations a uniform grid of 12x12x12 points was used. For the calculations of graphene a uniform grid of 8x8x1 points was used.

The six-dimensional integral in vdW-DF (see equation 2.6) samples the density on a real space grid [37]. The number of points in this grid can be set to something other than the default 2048 points. This was used in the bulk calculations where I set it to 4096 points.

The self-consistency loop ends when the density doesn't change much any more. Of course GPAW gives you the opportunity to define what "change much" means by setting the required *density accuracy*. By default the calculations are considered to be converged when the integrated magnitude of the change of the density is less than 10^{-4}. Since the van der Waals forces stem from small density redistributions near the atomic core, I chose to improve this default down to 10^{-5} when doing atomic relaxations with self-consistent vdW-DF.

In the same way one can set the required *eigenstate accuracy*. This is measured as the sum of the integrated magnitudes of the changes of all the wave functions from one cycle to the next. The default value for this parameter is 10^{-9}.

There are also several settings and parameters which I have not changed from their default values in any of the calculations, but let's not get into those. My choices of the parametres that are solely related to convergence (mixer settings and eigensolver) are not presented.

3.4 Test of noble gas setups

GPAW keeps PAW projectors and core states for the chemical elements in so called *setup*-files. When I started with this work, GPAW did not include PAW setups for all the noble gas atoms. Notably radon was missing. Marcin Dulak (Department of Physics, Technical University of Denmark), who is one of the developers of GPAW, kindly sent me his experimental noble gas setups. He has performed some preliminary tests of the setups but more tests would be needed before they can be officially included in GPAW [38].

For all the non noble gas elements I have used the setups from the latest version of the official GPAW setups pack. That is version 0.6.6300.

3.4.1 Noble gas bulk calculations

The setups that come with GPAW have been thoroughly tested by the developers and users, but the noble gas setups that I got have so far only gone through some of these tests. This led me to perform some tests of my own to ensure that they seemed physically sound.

To begin with, I have tested the crystal lattice structures for these setups. For each noble gas I set up a primitive unit cell for an FCC lattice (see figure 3.1) and calculated the energy for different lattice parameters. The minimum of

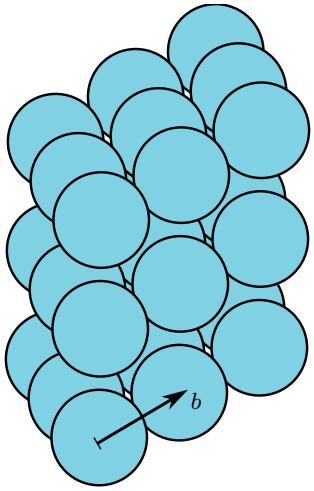

Figure 3.1: Crystal structure of solid argon. The picture shows 3x3x3 primitive unit cells. The vector b illustrates the nearest neighbour distance. The lattice parametre is then $a = \sqrt{2}b$.

this energy curve gave me the equilibrium lattice parameter for each element. The result of these calculations can be seen in table 4.1

For these bulk calculations I set a grid spacing of 0.07 Å. I used 12x12x12 k-points, six bands, and set the convergence criterion for eigenstates to 10^{-12}. The self consistent density was calculated using PBE and inserted into vdW-DF and vdW-DF2. Both of the van der Waals density functionals were calculated using 4096 real space points.

3.5 Adsorption on molecules

No interactions between the molecules have been considered. Instead, all calculations have been performed on single molecules.

Before I did any calculations on the molecules from tobacco they were relaxed until all forces were less than 50 meV/Å. The atomic relaxations were performed using revPBE to ensure that the molecule was in it desired configuration. The molecule was fixed in its relaxed configuration and the radon atom was introduced. This was done under the assumption that the adsorption of the radon atom doesn't affect the molecule's structure.

On some molecules I used self-consistent calculations to get the energy of the adsorbed system, and in other cases I used non self-consistent calculations. The details how these different calculations were performed, and which type of calculations I used when can be seen in the following sections.

3.5.1 Reference energies

To get a binding energy we also need reference energies for the free atom and molecule. This reference energy should in principle be calculated with the molecule and radon atom at infinite separation. This is of course not possi-

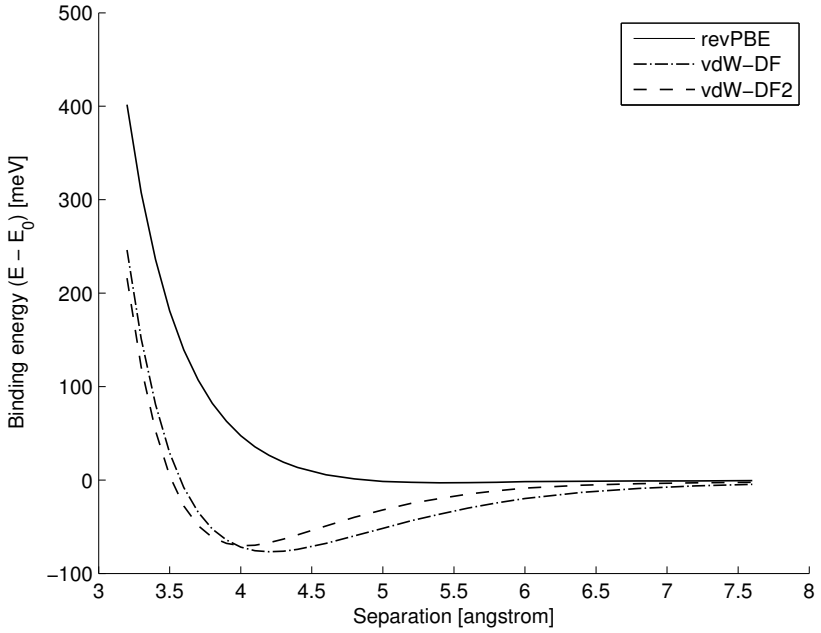

Figure 3.2: Binding energy curves for radon adsorption on benzene. The result for three different exchange correlation functionals can be compared. Note that revPBE gives almost no binding at all.

ble. Instead I have calculated the energy of a unit cell containing only one radon atom, and one containing only the molecule in question. The binding energy can then be calculated according to

$$E(R) = E_{\mathrm{both}}(R) - E_{\mathrm{mol}} - E_{\mathrm{Rn}}(R)\,. \tag{3.1}$$

In the case of non self-consistent calculations I have found the optimal (minimum energy) position by evaluating the equation 3.1 at several different separations R, and then by inspection finding the minimum of that graph. An example of such an energy curve can be seen in figure 3.2.

The reference energy for the molecule as well as for the free radon atom should in theory be independent of its position in the unit cell, so one might think that the term $E_{\mathrm{Rn}}(R)$ should not have a dependence on R. But because of the finite grid spacing, finite cell size etc. the energy differs slightly at different positions. Because of this I have calculated all reference energies with the atoms in the same positions as in the corresponding full calculation. Then the major part of these numerical errors should cancel.

In the case of self-consistent calculations the reference energy for the molecule was calculated in the same unit cell with the molecule in the same configuration as after the relaxation, but without the radon atom. And likewise for the radon atom, without the molecule. More about these calculations later on.

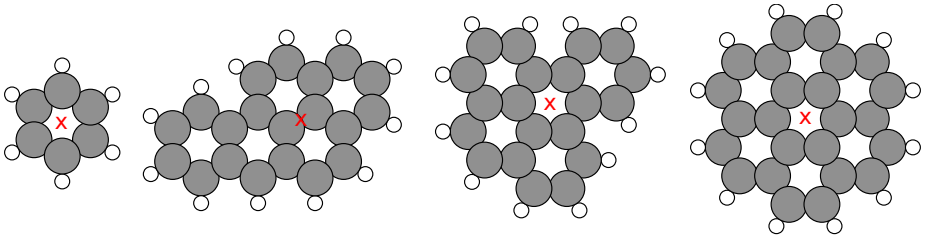

Figure 3.3: The different PAH molecules that I have done calculations on. Left to right: benzene, benzo[a]pyrene, benzo[e]pyrene, coronene. The white circles are hydrogen atoms and the grey ones represent carbon atoms. On all molecules except benzo[a]pyrene, the x shows the adsorption site that I have used. For benzo[a]pyrene the x instead shows the most favourable adsorption site.

3.6 Adsorption on PAH molecules

On these molecules I have performed non self-consistent calculations of the adsorption energy as it is the fastest way, and since I don't do any atomic relaxation the self-consistent vdW-DF isn't needed [20].

3.6.1 Noble gases on benzene

The next test for the setups was noble gas adsorption on benzene. These calculations were done with parameters very close to those used in all the other calculations. They were done non self-consistently for separations between 3 and 8 Å. An example of the kind of energy curve that results from these calculations can be seen in figure 3.2. A cell of dimensions 15x15x25 Å was used in which the benzene molecule was placed 10 Å from the $z = 0$ boundary.

This is also an interesting set of calculations in their own right. Their result can be seen in tables 4.2 and 4.3.

3.6.2 Radon on PAH

Apart from benzene, radon adsorption was calculated of three other PAH molecules, namely benzo[a]pyrene, benzo[e]pyrene and coronene. In figure 3.3 the different PAH molecules can be seen as well as the adsorption sites of the radon atom.

A cell of dimensions 16x16x25 Å was used in which the PAH molecule was placed 10 Å from the $z = 0$ boundary.

3.6.3 Radon on graphene

With several PAH molecules of different sizes we will be able to see how the molecule's size affects the binding. As a next step in this investigation I have chosen to look at radon binding on graphene.

This calculation was done very similiarly to the calculations of PAH molecules. I built a cell with 60 carbon atoms as seen in figure 3.5. Periodic boundary conditions were used in the x- and y-directions. As with the PAH molecules the cell

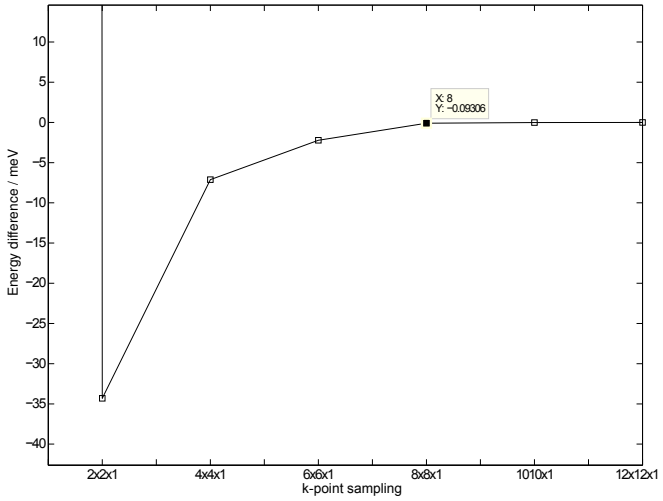

Figure 3.4: k-point convergence test for a unit cell of graphene as seen in figure 3.5. The reference energy is taken as the energy at 12x12x1 k-points. With too few k-points the energy varies alot, but as the number of k-points exceeds 8x8x1 the energy only changes about 0.1 meV.

was 25 Å in the z-direction and the graphene sheet was positioned 10 Å from the $z = 0$ plane.

With a metallic surface such as graphene the k-space sampling becomes very important. To ensure that I have a dense enough sampling I have performed a k-point convergence test. In figure 3.4 we can see that increasing the number of k-points beyond 8x8x1 doesn't affect the energy more than about 0.1 meV. I have thus chosen to do all calculations of radon on graphene with 8x8x1 k-points.

The results of these calculations can be seen in tables 4.3 and 4.3.

3.6.4 Site dependence on PAH

For the benzo[a]pyrene I performed a suite of calculations to test the site dependence of the physisorption of radon. In these calculations I fixed the radon atom in the x- and y-directions, and let it relax in the z-direction. This was done for a grid of 10x13 points in the x-y-plane.

It turned out that the easiest way to get convergence for the radon reference calculations was to do non self-consistent calculations. Because of this I also had to calculate the energy of the adsorbed system non self-consistently.

The result of these calculations can be seen in figure 4.1.

3.7 Radon on nitrosamines and nicotine

Two tobacco specific nitrosamines and nicotine were used. Pictures of these three molecules can be seen in figure 3.6.

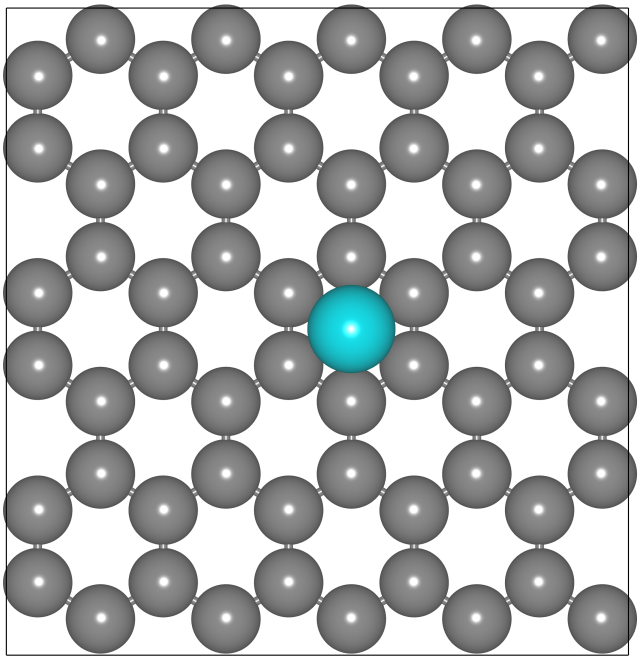

Figure 3.5: Radon atom adsorbed on graphene. Picture created using VESTA [1].

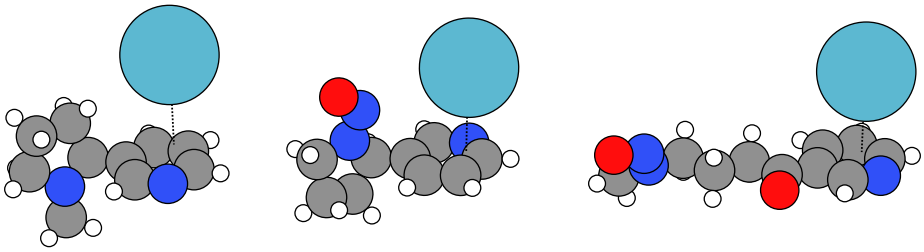

Figure 3.6: The nitrosamines and nicotine with radon adsorbed. Left to right: nicotine, NNN, NNK. The white circles are hydrogen atoms, red is oxygen, blue is nitrogen, grey is carbon and cyan is radon. The dotted line is meant to be orthogonal to the plane of the pyridine (C_5H_5N) group and is there to help interpret the position of the radon atoms relative to the molecules.

With a larger configuration space it was more difficult to find the spot where the radon atom would prefer to be. This led me to perform a new atomic relaxation where only the the newly introduced radon atom was free to move. This is only possible using the self-consistent version of the van der Waals density functional. These relaxations were performed until the forces on the radon atom were less than 5 meV/Å. The relaxed positions of the radon atoms is indicated in figure 3.6. The relaxation of the radon atom was done in a unit cell with 6 Å of vacuum in each direction. In all these calculations I increased the density accuracy to 10^{-5}.

In all the calculations I put the radon atom close to the pyridine group (see figure 3.6). This was because I wanted to test the difference in binding on the same group in different molecules.

The results of these calculations can be seen in tables 4.3 and 4.3.

Chapter 4

Results

In this chapter I will present the results of my calculations.

4.1 Test of noble gas setups

In table 4.1 the calculated lattice parameters for different noble gases can be compared with experimental values. As can be seen in table 4.1, using vdW-DF2 the lattice constants for argon, xenon, and krypton are correct to within about 2% of experimental values. The lattice constants with vdW-DF are correct to within about 7% of the experimental values. No experimental value for the lattice constant of radon exists to the best of my knowledge.

In table 4.2 the binding distances between benzene and different noble gases can be seen, as well as a comparison with experimental data. The binding energy of these systems can be seen in table 4.3.

The results in tables 4.1 and 4.2 show a fairly good agreement between calculations and experiments. The results in table 4.3 show a decent agreement between the calculations. The binding energies for these complexes varies alot in the literature, both between different calculations and between experiments, so the slightly bigger differences in energy than in distances is not all that worrying. These tests together with personal communication with Marcin Dulak [38] concerning the tests he has made for this set of noble gas setups makes me confident that the setups can be used in the further calculations.

Table 4.1: Lattice constants for noble gases. Experimental values are taken from Kittel [18].

	Calculated lattice constant (vdW-DF)	Calculated lattice constant (vdW-DF2)	Experimental value [18]
Ar	5.6 Å	5.3 Å	5.32 Å
Kr	6.0 Å	5.7 Å	5.67 Å
Xe	6.6 Å	6.3 Å	6.15 Å
Rn	6.8 Å	6.5 Å	

Table 4.2: Binding distances for benzene-Ng, with Ng $\in \{Ar, Kr, Xe, Rn\}$. Experimental values are from [39].

	Calculated binding distance (vdW-DF)	Calculated binding distance (vdW-DF2)	Experimental value [39]
Ar	3.8 Å	3.6 Å	3.50 Å
Kr	4.0 Å	3.7 Å	3.61 Å
Xe	4.1 Å	3.9 Å	3.77 Å
Rn	4.2 Å	4.0 Å	

Table 4.3: Binding energies for benzene-Ng, with Ng $\in \{Ar, Kr, Xe, Rn\}$. The last column shows the binding energy as calculated in [40], where empirical binding energy curves are fitted to non-empirical second-order Møller-Plesset calculations.

	Calculated binding energy (vdW-DF)	Calculated binding energy (vdW-DF2)	MP2 calculations [40]
Ar	-61.2 meV	-50.6 meV	-52.8 meV
Kr	-67.1 meV	-58.1 meV	-60.1 meV
Xe	-75.6 meV	-68.3 meV	-74.5 meV
Rn	-76.8 meV	-70.3 meV	

4.2 Adsorption sites on benzo[a]pyrene

In figure 4.1 the adsorption energy at different sites on a benzo[a]pyrene molecule can be seen. A big portion of the molecule exhibits significant adsorption which means that an adsorbed atom is free to move around somewhat on the surface of the molecule. In other words the radon atom can be seen as being adsorbed to the molecule rather than to any specific atom in the molecule. This should be noted as an important difference to some types of chemical bonds, such as covalent bonds.

4.3 Summary of adsorption energies and distances

The binding energy curve for radon on graphene can be seen in figure 4.2. As can also be noted in figure 3.2, revPBE gives almost no van der Waals binding at all. A summary of the binding energies of radon on different molecules can be found in table 4.3. In no case was there any barrier for adsorption, and no chemisorption well was found for any molecule.

For the case of radon on NNN and nicotine the adsorption sites didn't change much between vdW-DF and vdW-DF2. In the case of nicotine the difference in position was less than 0.01 Å and on NNN the difference is 0.064 Å. For NNK the radon atom was 0.336 Å closer to the pyridine (C_5H_5N) group, which is in line with the trends seen in table 4.2 and 4.3.

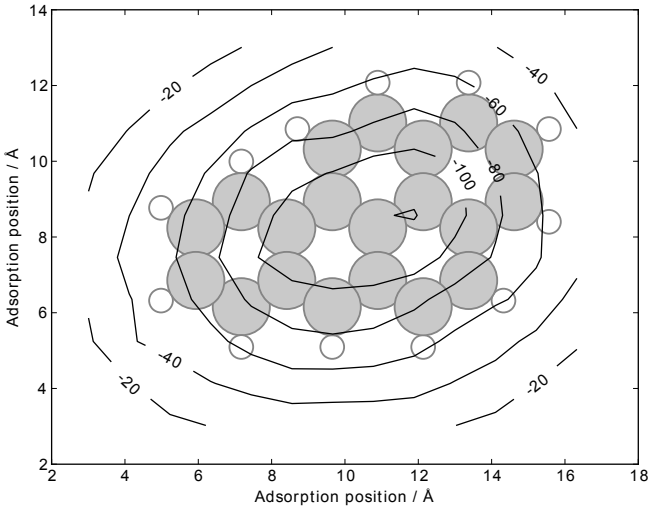

Figure 4.1: Adsorption energy at different sites on the benzo[a]pyrene molecule. The contour levels are in meV. The minimum value is -121 meV. The grey circles represent the carbon atoms and the white ones correspond to the hydrogen atoms. The positions of the atoms are correctly overlaid to within about 0.2 Å.

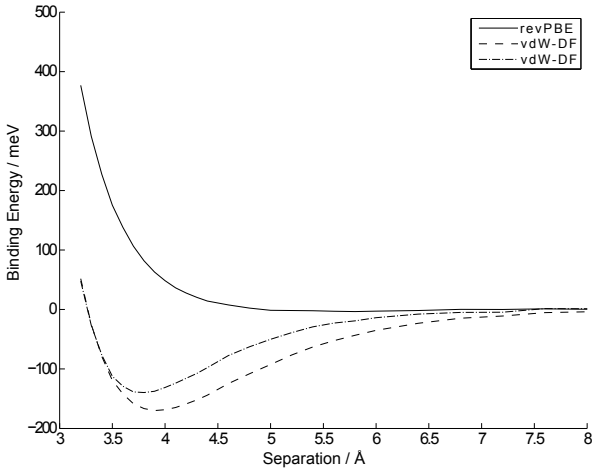

Figure 4.2: Binding energy for radon on graphene. The system can be seen in figure 3.5. Once again we see that revPBE gives almost no binding at all.

Table 4.4: Calculated adsorption energy for radon on different molecules. The computational parameters and other details of how these calculations were performed can be found in chapter 3.

Molecule	Binding energy (vdW-DF)	Binding energy (vdW-DF2)
Benzene	-77 meV	-70 meV
Benzo[e]pyrene	-146 meV	-127 meV
Benzo[a]pyrene		-121 meV
Coronene	-156 meV	-134 meV
Graphene	-170 meV	-140 meV
NNN	-102 meV	-84 meV
NNK	-88 meV	-80 meV
Nicotine	-87 meV	-78 meV

Table 4.5: Calculated adsorption distances for radon on different PAH molecules and graphene. The computational parameters and other details of how these calculations were performed can be found in chapter 3.

Molecule	Binding distance (vdW-DF)	Binding distance (vdW-DF2)
Benzene	4.2 Å	4.0 Å
Benzo[e]pyrene	4.0 Å	3.8 Å
Benzo[a]pyrene		3.9 Å
Coronene	3.9 Å	3.8 Å
Graphene	3.9 Å	3.8 Å

Chapter 5

Discussion and outlook

This thesis can only reasonably aim at solving one small piece of the puzzle that understanding the radon smoke correlation presents. That piece is the question of whether radon adsorbs on smoke molecules. The answer to this question seems to be *yes*. On all the molecules that I have investigated adsorption wells of between 70 meV and 156 meV were found.

It is important that the adsorption well is deep enough so that atoms don't fall out of it. The fact that there is no energy barrier for entering the adsorbed state makes this easier. In the equilibrium thermodynamics at room temperature the depth of the energy well is to be compared with the energy $k_B T = 25\,\text{meV}$. In all the molecules I have tested, the well is significantly deeper than this, which means that the binding is strong enough to hold at room temperature.

5.1 Size of molecules and atoms

In table 4.3 we can see that bigger PAH-molecules have stronger adsorption. This is not at all surprising considering that the van der Waals force is strictly attractive and relatively long range. For a larger systems more atoms will lay in the region of van der Waals attraction which will add up to a larger net attractive force.

This means that the amount of big PAH molecules in the smoke seem to be an important factor to consider when discussing radon inhalation. The amount of PAH molecules in tobacco smoke differs depending on a lot of different factors. PAH content has for example been found to correlate negatively with filtering [41][42]. Other factors such as tobacco curing and smoking conditions (longer/shorter and more/less frequent puffs) also seem to affect the amount of PAH [41][42].

Not only the size of the molecule but also the size of the atom seems to be of importance. In the London formula for the van der Waals binding energy 1.1, the coefficient C_6 is proportional to the polarisability of the atoms or molecules in question. An order of magnitude estimate of the polarisability of the atom (see for example Atkins et al. [43], chapter 8) tells us that the polarisability of the atom grows as the third power of the radius of the atom.

This trend can also be seen in table 4.3. The bigger the atom the deeper

the energy well. Since radon is the biggest of all the naturally occurring noble gases it is very van der Waals-reactive. It seems that the view point of radon as an inert gas with no interactions is a big simplification.

5.2 vdW-DF

The fact that no chemisorption wells were found on any of the molecules indicate that, as suspected, we need van der Waals interactions to be able to model these kinds of systems. Overall DFT with the vdW-DF is a robust and versatile tool for a huge variety of atomic simulations. Together with the very user-friendly environment ASE it is sure to be a weapon of choice for physicist and chemists alike for many years to come.

The newer version of the van der Waals-density functional gives consistently shorter binding distances than the older version. This behaviour is consistent also with other studies [30][44]. It would be very interesting to compare these results with other calculations done with other implementations of the density functional theory as well as with other methods of accounting for the van der Waals interactions.

In the case of bulk noble gases (see table 4.1) as well as in the case of noble gases on benzene (see table 4.2 and table 4.3) vdW-DF2 gives more accurate results compared to experiments.

5.3 Outlook

There are several directions that a future study might take.

One important step is to do thorough tests of the setups, including cross-referencing the results with known-to-work setups from other implementations of PAW.

As I mentioned, I have only investigated one aspect of the radon inhalation scenario, i.e. whether the radon atoms adsorbs on the molecules and if so with what binding energy. There are many other aspects of this model that need to be investigated before we can draw any conclusions on whether this kind of adsorptions can be responsible for the connection between tobacco smoking and radon related lung cancer risk.

One such example is a statistical model of the different paths of radon and its daughters into the lungs. For each of the different ways for radon and its daughters to get into the lung, one should be able to estimate the number of ^{222}Rn and ^{210}Pb atoms that end up in the lungs. In turn, from these numbers one should be able to estimate the amount of α-radiation that is suffered as well as the amount of radon-related lead accumulation. This could help pin point the most likely way for radon and its daughters to end up decaying in the lung, for smokers, passive smokers and non-smokers alike. This would indeed be very interesting.

One could also aim for experimental verification of these figures. Using DFT and PAW one can calculate ionisation energies of the core electrons in an atom. This ionisation energy can shift slightly depending on the atoms surroundings. It is not necessarily the case that vdW-forces suffice to give a core level shift. If there is a core level shift in the radon atom when it adsorbs it might be detectable

using for example XPS. As the theoretical emphasis in this thesis would seem to indicate, my knowledge in the potential experiments is unfortunately not sufficient to give any more information on their plausibility or on how they would be carried out.

Yet another direction that one might take is to investigate barriers for radon release. There is for example an isolation foam [45] originally developed as a moisture barrier for suspended basements. It has been noticed that this foam also catches the radon from the basement [46]. Preliminary studies show that for example epoxy paint can also be used as a radon barrier [46]. The non-empirical nature of DFT and vdW-DF permits similar simulations as the ones performed in this study to supplement and interpret experimental studies of such materials.

Bibliography

[1] Koichi Momma and Fujio Izumi. *VESTA*: a three-dimensional visualization system for electronic and structural analysis. *Journal of Applied Crystallography*, 41(3):653–658, Jun 2008.

[2] World Health Organization. Global burden of disease. `http://apps.who.int/ghodata/?vid=10012`, 2008.

[3] Hans Konrad Biesalski, Bas Bueno De Mesquita, Andrew Chesson, Frank Chytil, Robert Grimble, R. J. J. Hermus, Jochen Köhrle, Reuben Lotan, Karl Norpoth, Ugo Pastorino, and David Thurnham. European consensus statement on lung cancer: Risk factors and prevention, 1998.

[4] Agency for Toxic Substances & Disease Registry. Toxicological profile for radon. `http://www.atsdr.cdc.gov/ToxProfiles/tp.asp?id=407\&tid=71`, 2008.

[5] International Agency for Research on Cancer. Monographs on the evaluation of carcinogenic risks to humans: Man-made mineral fibres and radon. `http://monographs.iarc.fr/ENG/Monographs/vol43/volume43.pdf`, 1988.

[6] Swedish Radiation Safety Authority. Vägen till en radonfritt boende. `http://www.stralsakerhetsmyndigheten.se/Global/Publikationer/Broschyr/2009/Faktablad_Vagen_till_ett_radonfritt_boende2.pdf`, 2009.

[7] P. Gehr and J. Heyder. *Particle-lung interactions*. Lung biology in health and disease. M. Dekker, 2000.

[8] Swedish Radiation Safety Authority. Hur farligt är radon? `http://www.stralsakerhetsmyndigheten.se/Global/Publikationer/Broschyr/2009/faktablad-hur-farligt-ar-radon.pdf`, 2009.

[9] International Agency for Research on Cancer. Monographs on the evaluation of carcinogenic risks to humans: Inorganic and organic lead compounds. `http://monographs.iarc.fr/ENG/Monographs/vol87/volume87.pdf`, 2006.

[10] Agency for Toxic Substances & Disease Registry. Toxicological profile for lead. `http://www.atsdr.cdc.gov/ToxProfiles/tp.asp?id=96&tid=22`, 2007.

[11] R. L. Stedman. The chemical composition of tobacco and tobacco smoke. *Chemical Review*, 68(2):153–207, 1968.

[12] R. Doll and A. B. Hill. Smoking and carcinoma of the lung. *British Medical Journal*, pages 740–748, 1950.

[13] International Agency for Research on Cancer. Monographs on the evaluation of carcinogenic risks to humans: Tobacco smoking. `http://monographs.iarc.fr/ENG/Monographs/vol38/volume38.pdf`, 1986.

[14] World Health Organization. Report on the global tobacco epidemic. `http://www.who.int/tobacco/mpower/2009/gtcr_download/en/index.html`, 2009.

[15] EPA. Assessment of risks from radon in homes. `http://www.epa.gov/radiation/docs/assessment/402-r-03-003.pdf`, 2003.

[16] Kellar Autumn, Metin Sitti, Yiching A. Liang, Anne M. Peattie, Wendy R. Hansen, Simon Sponberg, Thomas W. Kenny, Ronald Fearing, Jacob N. Israelachvili, and Robert J. Full. Evidence for van der waals adhesion in gecko setae. *Proceedings of the National Academy of Sciences*, 99(19):12252–12256, 2002.

[17] K. Berland. Bound by long-range interactions: Molecular crystals and benzene on cu(111). Licentiate thesis, 2009.

[18] C. Kittel. *Introduction to Solid State Physics*. John Wiley & Sons, Inc., eighth edition, 2005.

[19] R. P. Feynman. Forces in molecules. *Physical Review*, 56(4):340–343, 1939.

[20] T. Thonhauser, V. R. Cooper, S. Li, A. Puzder, P. Hyldgaard, and D. C. Langreth. Van der waals density functional: Self-consistent potential ant the nature of the van der waals bond. *Physical Review B*, 76(12):125112, 2007.

[21] P. Hohenberg and W. Kohn. Inhomogeneous electron gas. *Physical Review*, 136(3B):B864–B871, 1964.

[22] R. M. Martin. *Electronic Structure*. Cambridge University Press, 2005.

[23] W. Kohn and L. J. Sham. Self-consistent equations including exchange and correlation effects. *Physical Review*, 140(4A):A1133–A1138, 1965.

[24] John P. Perdew, Kieron Burke, and Matthias Ernzerhof. Generalized gradient approximation made simple. *Physical Review Letters*, 77(18):3865–3868, Oct 1996.

[25] J. P. Perdew, K. Burke, and M. Ernzerhof. Generalized gradient approximation made simple [phys. rev. lett. 77, 3865 (1996)]. *Physical Review Letters*, 78(7):1396, Feb 1997.

[26] Yingkai Zhang and Weitao Yang. Comment on "generalized gradient approximation made simple". *Physical Review Letters*, 80(4):890, Jan 1998.

[27] M. Dion, H. Rydberg, E. Schroder, D.C. Langreth, and B. I. Lundqvist. Van der waals density functional for general geometries. *Physical Review Letters*, 92(24):246401, 2004.

[28] M. Dion, H. Rydberg, E. Schroder, D.C. Langreth, and B. I. Lundqvist. Erratum: Van der waals density functional for general geometries. *Physical Review Letters*, 95:109902, 2005.

[29] S. Grimme. Density functional theory with london dispersion corrections. *Computational Molecular Science*, 1:211–228, 2011.

[30] K. Lee, É. D. Murray, L. Kong, B. I. Lundqvist, and D. C. Langreth. Higher-accuracy van der waals density functional. *Physical Review B*, 82(8):081101, 2010.

[31] P. E. Blöchl. Projector augmented-wave method. *Physical Review B*, 50:17953–17979, 1994.

[32] P. E. Blöchl. Projector augmented wave method: ab initio molecular dynamics with full wave functions. *Bulletin of Material Science*, 26(1):33–41, 2003.

[33] J. J. Mortensen, L. B. Hansen, and K. W. Jacobsen. Real-space grid implementation of the projector augmented wave method. *Physical Review B*, 71(25):035109, 2005.

[34] J. Enkovaara, C. Rostgaard, and J. J. Mortensen et al. Electronic structure calculations with gpaw: a real-space implementation of the projector augmented-wave method. *Journal of Physics: Condensed Matter*, 22(3):253202, 2010.

[35] S. R. Bahn and K. W. Jacobsen. An object-oriented scripting interface to a legacy electronic structure code. *Computing in Science and Engineering*, 4(3):56–66, 2002.

[36] GPAW. Convergence issues. `https://wiki.fysik.dtu.dk/gpaw/documentation/convergence/convergence.html`, fetched 2011-06-09.

[37] Guillermo Román-Pérez and José M. Soler. Efficient implementation of a van der waals density functional: Application to double-wall carbon nanotubes. *Physical Review Letters*, 103(9):096102, Aug 2009.

[38] Marcin Dulak. Personal communication, 2011.

[39] Th. Brupbacher, J. Makarewicz, and A. Bauder. Intermolecular dynamics of benzene-rare gas complexes as derived from microwave spectra. *Journal of Chemical Physics*, 101:9736–9746, 1994.

[40] P. Hobza, Ota Bludský, H. L. Selzle, and E. W. Schlag. Ab initio second- and fourth-order moller-plesset study on structure, stabilization energy, and stretching vibration of benzene...x (x=he,ne,ar,kr,xe) van der waals molecules. *Journal of Chemical Physics*, 97:335, 1992.

[41] Yan S. Ding, Xizheng J. Yan, Ram B. Jain, Eugene Lopp, Ameer Tavakoli, Gregory M. Polzin, Stephen B. Stanfill, David L. Ashley, and Clifford H. Watson. Determination of 14 polycyclic aromatic hydrocarbons in mainstream smoke from u.s. brand and non-u.s. brand cigarettes. *Environmental Science & Technology*, 40(4):1133–1138, 2006.

[42] Yan S. Ding, David L. Ashley, and Clifford H. Watson. Determination of 10 carcinogenic polycyclic aromatic hydrocarbons in mainstream cigarette smoke. *Journal of Agricultural and Food Chemistry*, 55(15):5966–5973, 2007.

[43] Peter Atkins, Julio de Paula, and Ronald Friedman. *Quanta, Matter, and Change: A molecular approach to physical chemistry.* Oxford University Press, 2009.

[44] E. Varenius. Hydrogen adsorption on graphene and coronene. Unpublished Master Thesis, 2011.

[45] Klimatzonen. www.klimatzonen.se.

[46] Göran Nyman. Personal communication, 2011.